Viscoelasticity of a homeotropic nematic slab

Patrick Oswald[*]

*Université de Lyon, Ecole Normale Supérieure de Lyon, Laboratoire de physique, CNRS, UMR5672, 46 Allée d'Italie,
69364 Lyon Cedex 7, France*

The viscoelastic behavior of a homeotropic nematic slab is studied when it is subjected to a (dilation-compression) sinusoidal deformation of small amplitude (linear regime). I show that the nematic phase behaves as an isotropic liquid of viscosity η_c (ν_3) at low (high) frequency, where η_c is the third Miesowicz viscosity and ν_3 a smaller viscosity first introduced by Martin, Parodi, and Pershan. The crossover frequency $f^\star$ between these two asymptotic regimes scales as h^2/D, where h is the sample thickness and $D = K_3/\gamma_1$ is the orientational diffusivity (with K_3 the bend constant and γ_1 the rotational viscosity). Between these two limits the sample behaves as a viscoelastic fluid whose elastic and loss moduli G' and G'' are calculated. These predictions are tested experimentally with a piezoelectric rheometer.

I. INTRODUCTION

In 1990, Okana and Yamamoto calculated [1] and measured experimentally [2] the mechanical transfer function of a nematic slab confined between two glass plates treated for strong homeotropic anchoring. "Strong" here means that the anchoring extrapolation length K/W_a first introduced by de Gennes [3] (where K is an elastic constant and W_a is the anchoring energy) is much smaller than the slab thickness. Their conclusion was that the slab behaves as a Newtonian viscous fluid of viscosity equal to the third Miesowicz viscosity η_c (defined when the director $\vec{n}$ is perpendicular to the velocity $\vec{v}$ and parallel to the velocity gradient $\vec{\nabla} v$). In terms of Leslie's coefficient α_i [3,4],

$$\eta_c = \tfrac{1}{2}(\alpha_4 + \alpha_5 - \alpha_2). \tag{1}$$

While trying to measure η_c with a piezoelectric rheometer, I realized that this result was only true at very low frequency and small thickness and that the sample usually behaves as a viscoelastic fluid of non-negligible elastic modulus G' with respect to its loss modulus G''. For this reason, I calculated G' and G'' from the equations of nematohydrodynamics to fit my experimental data. This allowed me to directly measure η_c, but also the diffusivity $D = K_3/\gamma_1$ and another viscosity,

$$\nu_3 = \eta_c - \frac{\alpha_2^2}{\gamma_1}, \tag{2}$$

first introduced by the Harvard group [3,5]. Here, K_3 is the bend elastic constant and $\gamma_1 = \alpha_3 - \alpha_2$ is the rotational viscosity.

II. THEORY

The nematic slab (of radius R and thickness $h \ll R$) is sandwiched between two parallel circular disks treated for strong homeotropic anchoring. The upper disk oscillates so that $h = h_0 + \delta h \cos(\omega t)$. The vibration amplitude is small enough ($\delta h \ll h_0$) in order to stay in the linear regime of deformation. For this reason and to simplify the notations, I

___

*patrick.oswald@ens-lyon.fr

replace h_0 by h in the following each time it is possible. The z axis is perpendicular to the plane of the disks situated at $z = \pm h/2$.

My purpose is to calculate the stress $\sigma(t) = \sigma' \cos(\omega t) - \sigma'' \sin(\omega t)$ that the nematic slab exerts on the upper plate by solving the equation of nematohydrodynamics. Let $\vec{n}$ be the director and $\vec{v}$ the velocity. In the linear regime, at first order in deformation, $\vec{n} = (n_x, n_y, 1)$ and $\vec{v} = (v_x, v_y, v_z)$. As $h \ll R$, $\partial/\partial z \gg \partial/\partial x$ and $\partial/\partial y$ so that $v_z \ll v_x$ and v_y according to the incompressibility condition $\vec{\nabla} \cdot \vec{v} = 0$ (lubrication approximation). In these conditions, the torque equation simplifies to

$$K_3 n_{x,zz} - \gamma_1 n_{x,t} - \alpha_2 v_{x,z} = 0, \tag{3}$$
$$K_3 n_{y,zz} - \gamma_1 n_{y,t} - \alpha_2 v_{y,z} = 0, \tag{4}$$

where the terms in K_3, γ_1, and α_2 respectively represent the restoring elastic torque, the viscous torque, and the hydrodynamic torque due to the flow. Note that in these equations, I neglected the splay term in $K_1(n_{i,xx} + n_{i,yy})$ with respect to the bend term in $K_3 n_{i,zz}$ ($i = x, y$) because $\partial^2/\partial x^2 + \partial^2/\partial y^2 \ll \partial^2/\partial z^2$ in the framework of the lubrication approximation.

Similarly, the momentum equation reads

$$\frac{\partial P}{\partial z} = 0, \tag{5}$$
$$\frac{\partial P}{\partial x} = \alpha_2 n_{x,zt} + \eta_c v_{x,zz}, \tag{6}$$
$$\frac{\partial P}{\partial y} = \alpha_2 n_{y,zt} + \eta_c v_{y,zz}, \tag{7}$$

where P is the pressure. As expected, these equations show that the director and velocity fields are coupled via the viscosity α_2 (indeed, if $\alpha_2 = 0$ the equations for $\vec{n}$ and $\vec{v}$ become independent).

To solve these equations together with the incompressibility condition $\vec{\nabla} \cdot \vec{v} = 0$, I assume a solution of the form

$$P = A(t)(x^2 + y^2 - R^2), \tag{8}$$
$$n_x = x f(z,t); \, n_y = y f(z,t), \tag{9}$$
$$v_x = x \, g(z,t); \, v_y = y \, g(z,t), \tag{10}$$

which has radial symmetry [in cylindrical coordinates $n_r = rf(z,t)$ and $v_r = rg(z,t)$]. In addition and for symmetry reasons, I assume that f (g) is odd (even) in z which implies that $f_{,z}$ ($g_{,z}$) is even (odd) in z. This property is used in the following.

I emphasize that this solution satisfies the boundary condition for the pressure at the free surface of the sample since $P = 0$ at $r = R$. Note here that I set the atmospheric pressure equal to zero. More importantly, I suppose that the jump of capillary pressure at the free surface is negligible. In practice, this condition is achieved by using a lower plate of larger radius than the upper plate. In this way, it is possible to fill the sample with a large excess of LC in order to create a bulge of LC of millimetric size around the sample. In these conditions, the capillary effects become negligible because the radius of curvature of the interface with the air is very large compared to the sample thickness.

As for the condition of homeotropic anchoring, it yields

$$f\left(\pm\frac{h}{2},t\right) = 0, \tag{11}$$

while the condition of no sliding of the fluid on the disks imposes

$$g\left(\pm\frac{h}{2},t\right) = 0. \tag{12}$$

I now solve these equations, noting that Eq. (5) is automatically satisfied with this choice of solution. Equations (6) and (7) give

$$2A = \alpha_2 f_{,zt} + \eta_c g_{,zz}, \tag{13}$$

and Eqs. (3) and (4) lead to

$$K_3 f_{,zz} = \gamma_1 f_{,t} + \alpha_2 g_{,z}. \tag{14}$$

Eliminating time between these two equations yields

$$2A = \frac{\alpha_2 K_3}{\gamma_1} f_{,zzz} + \nu_3 g_{,zz}, \tag{15}$$

where ν_3 is given by Eq. (2). Note that this viscosity is the one an experimentalist would measure if the director was free to rotate in the flow, i.e., in the absence of any elastic restoring torque ($K_3 = 0$). Integrating this equation twice with respect to z and putting the boundary condition (12), I obtain

$$g = \frac{A}{\nu_3}\left(z - \frac{h}{2}\right)\left(z + \frac{h}{2}\right) - \frac{\alpha_2 K_3}{\gamma_1 \nu_3}\left[f_{,z} - f_{,z}\left(-\frac{h}{2}\right)\right]. \tag{16}$$

I now express that the upper plate oscillates while the other is at rest. From the incompressibility condition and Eqs. (10), I obtain

$$v_z = -\int_{-\frac{h}{2}}^{z} 2g \, dz, \tag{17}$$

which gives by using Eq. (16)

$$v_z = -\frac{2A}{\nu_3}\left(\frac{z^3}{3} - \frac{h^2}{4}z - \frac{h^3}{12}\right) + \frac{2\alpha_2 K_3}{\gamma_1 \nu_3}\left[f - f\left(-\frac{h}{2}\right) - f_{,z}\left(-\frac{h}{2}\right)\left(z + \frac{h}{2}\right)\right]. \tag{18}$$

Writing that $v_z(h/2) = \dot{h}$ (where the dot denotes the derivative with respect to time) yields the pressure coefficient A:

$$A = \frac{3\nu_3 \dot{h}}{h^3} + \frac{6\alpha_2}{h^2}\frac{K_3}{\gamma_1}f_{,z}\left(-\frac{h}{2}\right). \tag{19}$$

The next step is to calculate f. Replacing g by its expression (16) in Eq. (14) gives

$$Dcf_{,zz} - f_{,t} + \frac{2kA}{\nu_3}z = 0, \tag{20}$$

where constants $c = \frac{\eta_c}{\eta_c + k\alpha_2} = \frac{\eta_c}{\nu_3}$ and $k = -\frac{\alpha_2}{\gamma_1}$ are two dimensionless numbers.

To solve this equation, I set $f(z,t) = f_1(z)\cos(\omega t) + f_2(z)\sin(\omega t)$, which gives after substitution into Eqs. (19) and (20)

$$A = -\left(\frac{3\nu_3}{h^2}\varepsilon\omega - 6\alpha_2\frac{D}{h^2}f_2'\right)\sin(\omega t) + 6\alpha_2\frac{D}{h^2}f_1'\cos(\omega t) \tag{21}$$

and

$$\begin{cases} Dcf_{1,zz} - \omega f_2 + 12\frac{k\alpha_2}{\nu_3}\frac{D}{h^2}f_1'z = 0, \\ Dcf_{2,zz} + \omega f_1 + \left(-\frac{6k}{h^2}\varepsilon\omega + 12\frac{k\alpha_2}{\nu_3}\frac{D}{h^2}f_2'\right)z = 0. \end{cases} \tag{22}$$

Here, $\varepsilon = \frac{\delta h}{h}$ is the deformation and $f_i' = f_{i,z}(\pm\frac{h}{2})$ ($i = 1,2$). The general solution of this system of equations reads

$$\begin{cases} f_1 = \left(\frac{6k}{h^2}\varepsilon - 12\frac{k\alpha_2}{\nu_3}\frac{D}{h^2}\frac{f_2'}{\omega}\right)z \\ \quad + E\cos(\alpha z)\sinh(\alpha z) + F\sin(\alpha z)\cosh(\alpha z), \\ f_2 = 12\frac{k\alpha_2}{\nu_3}\frac{D}{h^2}\frac{f_1'}{\omega}z \\ \quad - E\sin(\alpha z)\cosh(\alpha z) + F\cos(\alpha z)\sinh(\alpha z), \end{cases} \tag{23}$$

where $\alpha = \sqrt{\frac{\omega}{2cD}}$.

The next step is to calculate the four constants f_1', f_2', E, and F. This can be done by expressing that $f_1(h/2) = f_2(h/2) = 0$ and by calculating f_1' and f_2' from the previous system of equations. This procedure gives

$$\begin{cases} \beta h f_2' + E\cos u \sinh u + F\sin u \cosh u = -3k\frac{\varepsilon}{h}, \\ \beta h f_1' + E\sin u \cosh u - F\cos u \sinh u = 0, \\ -f_1' + 2\beta f_2' + E\alpha(-\sin u \sinh u + \cos u \cosh u) \\ \quad + F\alpha(\sin u \sinh u + \cos\cosh u) = -6k\frac{\varepsilon}{h^2}, \\ 2\beta f_1' + f_2' + E\alpha(\sin u \sinh u + \cos u \cosh u) \\ \quad + F\alpha(\sin u \sinh u - \cos u \cosh u) = 0, \end{cases} \tag{24}$$

where $u = \alpha \frac{h}{2} = \sqrt{\frac{\bar{\omega}}{8(1-k\alpha_2/\nu_3)}}$, $\beta = -6\frac{k\alpha_2}{\nu_3}\frac{1}{\bar{\omega}}$, and $\bar{\omega} = \frac{\omega}{D/h^2}$ is the dimensionless frequency. Solving this system of equations

with MATHEMATICA allows me to explicitly calculate f_1' and f_2':

$$\begin{cases} \dfrac{f_1'}{\varepsilon} = -\dfrac{6k(\cos(2u) - \cosh(2u) + u\sin(2u) + u\sinh(2u))}{h^2((-1 + (-4 + 8u^2)\beta^2)\cos(2u) + (1 + (4 + 8u^2)\beta^2)\cosh(2u) - 4u\beta((-1 + 2\beta)\sin(2u) + (1 + 2\beta)\sinh(2u)))}, \\[4mm] \dfrac{f_2'}{\varepsilon} = \dfrac{6k(2(1 - 2u^2)\beta\cos(2u) - 2(1 + 2u^2)\beta\cosh(2u) + u(-1 + 4\beta)\sin(2u) + u(1 + 4\beta)\sinh(2u))}{h^2((-1 + (-4 + 8u^2)\beta^2)\cos(2u) + (1 + (4 + 8u^2)\beta^2)\cosh(2u) - 4u\beta((-1 + 2\beta)\sin(2u) + (1 + 2\beta)\sinh(2u)))}. \end{cases}$$

(25)

Finally, the stress σ that the nematic slab exerts on the upper plate can be calculated by noting that the viscous stress and the Eriksen elastic stress are negligible (of second order in deformation):

$$\sigma = \frac{1}{\pi R^2}\int_0^R -A(r^2 - R^2)2\pi r\, dr = \frac{1}{2}AR^2,$$

(26)

where A is given by Eqs. (21) and (25). Finally, the effective elastic and loss moduli of the nematic slab (effective because they depend not only on the anchoring condition, here homeotropic, but also on the sample thickness h) can be calculated by using the classical formulas for a viscoelastic fluid [6]:

$$\sigma = \frac{3}{2}\left(\frac{R}{h}\right)^2\varepsilon[G'\cos(\omega t) - G''\sin(\omega t)].$$

(27)

By identification, I obtain

$$G' = 2\alpha_2 D\frac{f_1'}{\varepsilon},$$

(28)

$$G'' = \nu_3\omega - 2\alpha_2 D\frac{f_2'}{\varepsilon},$$

(29)

where f_1'/ε and f_2'/ε are given by Eq. (25). A remarkable fact is that G' and G'' only depend on three constants of the nematic phase, namely, the diffusivity D and the two viscosities ν_3 and $k\alpha_2$ or, equivalently, D and the two viscosities η_c and ν_3 as $\eta_c = \nu_3 - k\alpha_2$. Another interesting point is to note that $G' \to 0$ and $G'' \to \eta_c\omega$ when $\omega \to 0$ while $G' \to \frac{3}{\sqrt{2}}k\alpha_2\sqrt{\frac{\nu_3}{\eta_c}}\sqrt{\omega\frac{D}{h^2}} \propto \sqrt{\omega}$ and $G'' \to \nu_3\omega$ when $\omega \to \infty$. This shows that the nematic phase behaves as an isotropic liquid of viscosity ν_c at low frequency and a liquid of viscosity ν_3 at large frequency (because, in this limit, G' becomes negligible with respect to G''). In between these two asymptotic regimes, the nematic phase behaves as a viscoelastic fluid. This viscoelastic behavior can be explained qualitatively as follows: because of the flow, the director field is deformed [term in α_2 in the torque equations (3) and (4)]. Because of the curvature elasticity this deformation tends to relax which induces a backflow and hence a modification of the pressure field [term in α_2 in the momentum equations (6) and (7)] responsible for the elastic behavior of the nematic phase.

To illustrate these results, I plotted in Fig. 1 the two moduli G' and G'' and their ratio G'/G'' as a function of the angular frequency for a "thin" and a "thick" nematic slab (of thickness $h = 20$ μm and $h = 200$ μm, respectively) by taking $\nu_3 = 0.04$ Pa s, $k\alpha_2 = -0.1$ Pa s (which gives $\eta_c = 0.14$ Pa s), and $D = 1 \times 10^{-10}$ m^2 s^{-1}.

As we can see in Fig. 1(c), the ratio G'/G'' passes through a maximum at a crossover frequency $\omega^\star$ which scales like D/h^2 times a function of the viscosities. This function (of the order of 100 here) is impossible to calculate analytically, although the ratio G'/G'' is written in the simple form

$$\frac{G'}{G''} = \frac{2\beta(\cos(2u) - \cosh(2u) + u\sin(2u) + u\sinh(2u))}{-\cos(2u) + \cosh(2u) + 2u\beta\sin(2u) - 2u\beta\sinh(2u)},$$

(30)
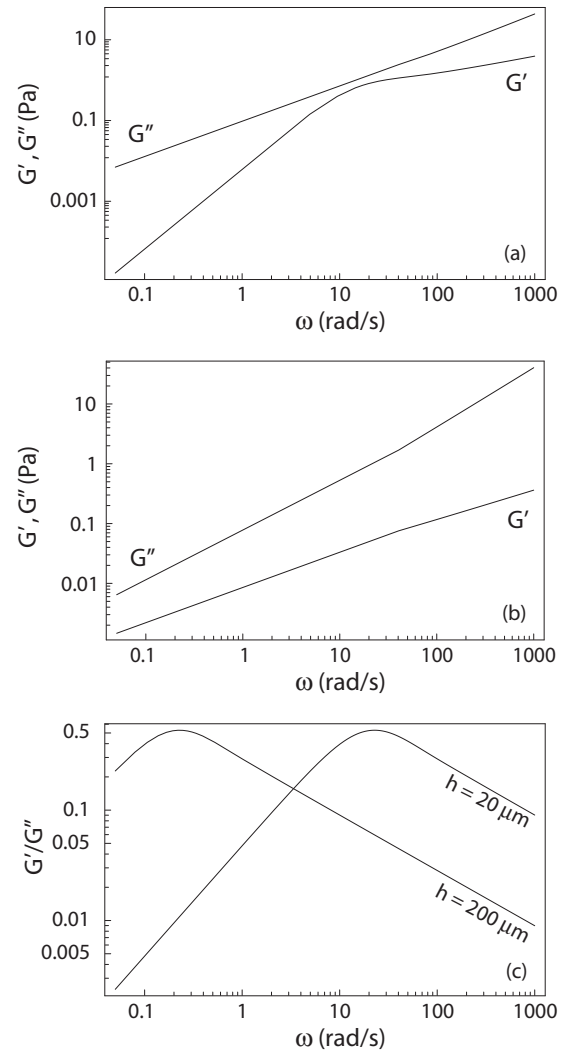
FIG. 1. Elastic and loss moduli as a function of frequency for two nematic slabs of thickness (a) $h = 20$ μm and (b) $h = 200$ μm, and (c) their ratios as a function of frequency.
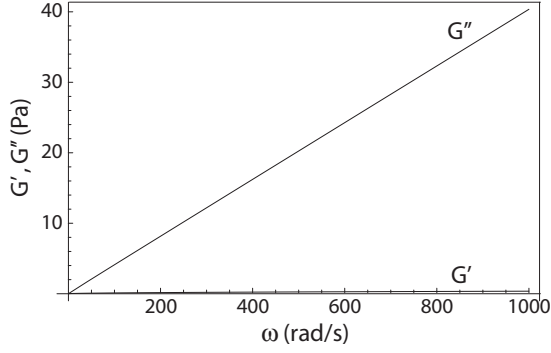
FIG. 2. The same data as in Fig. 1(b) in linear scale for $h = 200\ \mu$m. The figure shows that G' is too small to be measured while G'' varies linearly as a function of ω as expected for a Newtonian viscous fluid (with $G'' \approx \nu_3 \omega$). These curves are quite similar to the experimental curves shown in Fig. 3 of Ref. [2].

where $u \propto \sqrt{\omega}$ and $\beta \propto 1/\omega$ have been defined above.

Figure 1 also shows that in the range of frequencies accessible experimentally (between 5 and 500 rad/s with my rheometer; see the next section), the change of regime is only visible in very thin slabs of thickness $h < 30\ \mu$m. At larger thickness, G' becomes negligible with respect to G'' as one can see better in Fig. 2 where I plotted the same data as in Fig. 1(b) in linear scale. This remark allows me to explain the previous

experimental results of Yamamoto and Okano [2], who found a Newtonian behavior in a thick sample of homeotropic nematic phase. I nonetheless insist on the fact that these authors did not measure η_c (as they claim in Ref. [1]), but ν_3.

For completeness, I also plot in Fig. 3 the functions $f(z,t)/\epsilon = n_r(z,t)/(\epsilon r)$ and $g(z,t)/\epsilon = v_r(z,t)/(\epsilon r)$ over a half-period of time ($0 \leqslant \omega t \leqslant \pi$, knowing that during the next half-period these functions only change sign) at three different frequencies by taking $h = 20\ \mu$m (as in my experiments) and $k = 1$ (with the same values as above for D, η_c, ν_3, and α_2). The origin of time is given by the relation $h = h_0 + \epsilon h_0 \cos(\omega t)$. The curves in Figs. 3(a) and 3(b) were calculated at very low frequency (0.2 rad/s) with respect to $\omega^\star$, the curves in Figs. 3(c) and 3(d) at the frequency $\omega^\star$ at which the ratio G'/G'' passes through a maximum [$\omega^\star \approx 22.8$ rad/s, see Fig. 1(c)], and the curves in Figs. 3(e) and 3(f) at large frequency with respect to $\omega^\star$ (2000 rad/s). These curves show that the velocity profile is parabolic at low frequencies and tends to become again parabolic at large frequencies. On the other hand, it shifts significantly from the parabolic profile in the intermediate regime, when ω is close to $\omega^\star$. These curves also show that the tilt angle of the director tends to zero when $\omega \to 0$ and becomes significant when $\omega \sim \omega^\star$ or larger. An interesting observation is that the maximum tilt angle is obtained at $z = \pm 0.3h$ at the crossover frequency $\omega^\star$ and shift towards the two surfaces when the frequency increases without changing
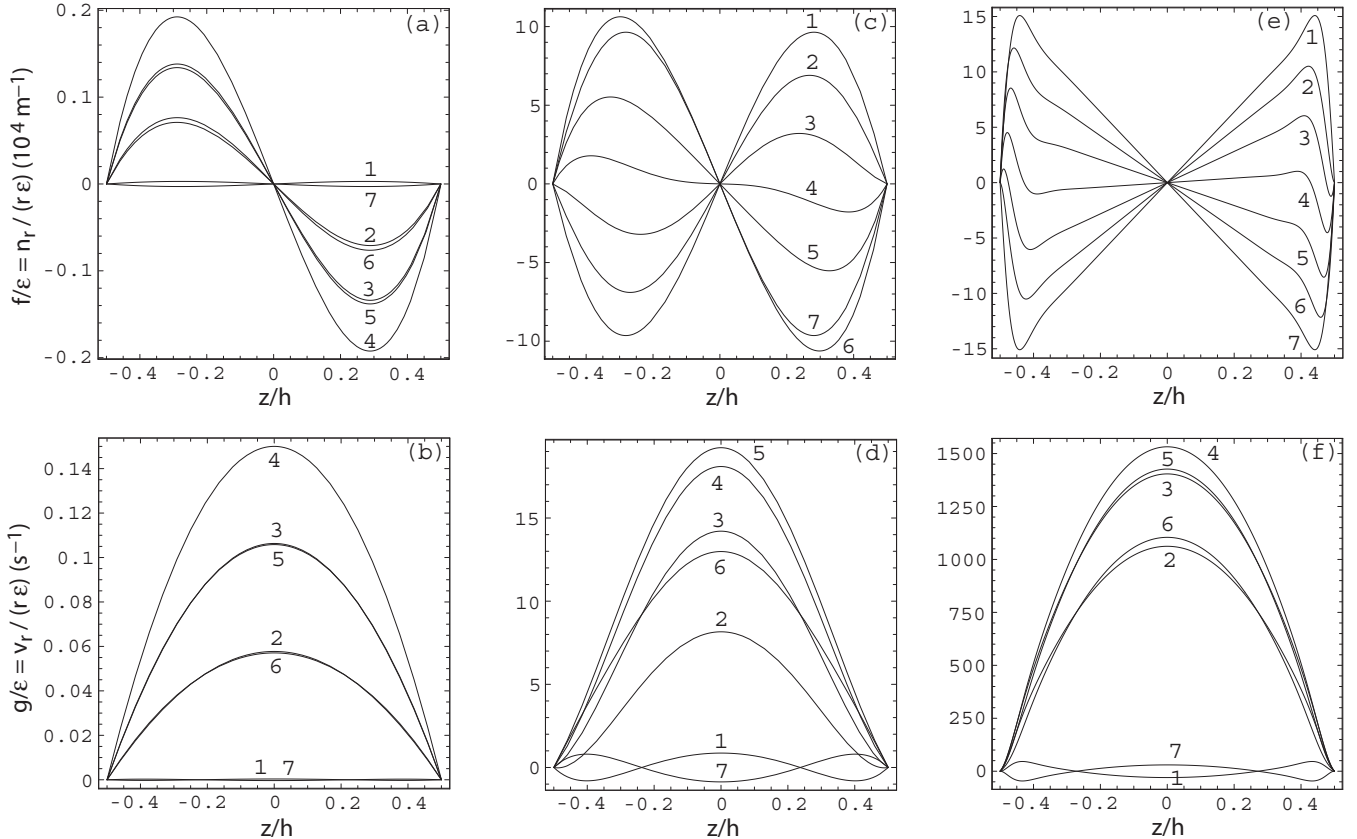
FIG. 3. (a,c,e) Director and (b,d,f) velocity profiles calculated numerically in a thin sample ($h = 20\ \mu$m) at three different frequencies: (a,b) 0.2 rad/s, (c,d) 22.8 rad/s, and (e,f) 2000 rad/s. The curves numbered from 1 to 7 have been calculated at particular times ωt in order that the curves f are regularly spaced. In (a,b), curves 1–7 correspond to times $\omega t = 0, \frac{\pi}{8}, \frac{\pi}{4}, \frac{\pi}{2}, \frac{3\pi}{4}, \frac{7\pi}{8}$, and π; in (c,d), times are $\omega t = 0, \frac{\pi}{8}, \frac{\pi}{4}, \frac{3\pi}{8}, \frac{\pi}{2}, \frac{3\pi}{4}$, and π; in (e,f), times are $\omega t = 0, \frac{\pi}{4}, \frac{3\pi}{8}, \frac{\pi}{2}, \frac{5\pi}{8}, \frac{3\pi}{4}$, and π.

significantly. This leads to the formation of a boundary layer at large frequency [of thickness δ of the order of $0.1h$ at 2000 rad/s; see Fig. 3(e)] inside which the tilt angle returns to zero. At this level, it must be noted that the condition for strong homeotropic anchoring is satisfied provided that the anchoring extrapolation length is smaller than δ—and not h—which is more restrictive. These graphs also give the order of magnitude of the velocity and of the director tilt angle at the edge of the sample at $r = R$. For instance, $v_r^{\max} \approx 9.5$ μm/s and $n_r^{\max} \approx 0.053$ rad $= 3°$ at $\omega = 22.8$ rad/s by taking $R = 5$ mm and $\epsilon = 1 \times 10^{-4}$. Another interesting point is the linear behavior of $f(z)$ at large frequency in the middle of the sample. This behavior can be easily found from Eqs. (3) and (4) by noting that at large frequencies the elastic term is negligible with respect to the viscous terms in the middle of the sample. This gives $n_{r,t} = -(\alpha_2/\gamma_1)v_{r,z}$ or equivalently $f_{,t} = -(\alpha_2/\gamma_1)g_{,z}$. At these frequencies the velocity profile is almost parabolic, of expression $g/\epsilon = -(3/h^2)(z - h/2)(z + h/2)\omega \sin(\omega t)$. This gives $f/\epsilon = -(6\alpha_2)/(\gamma_1 h^2)z \cos(\omega t)$ in the middle of the sample as observed in Fig. 3(e). In a similar way, it is possible to calculate f at low frequencies. In this limit, the term in γ_1 becomes negligible with respect to the term in K_3 in Eqs. (3) and (4). This gives $K_3 n_{r,z} = \alpha_2 v_r + C$ or, equivalently, $f_{,z} = (\alpha_2/K_3)g + C$, where C is a constant. With $g/\epsilon = -(3/h^2)(z - h/2)(z + h/2)\omega \sin(\omega t)$, I finally calculate $f/\epsilon = -(3\alpha_2)/(K_3 h^2)(z^3/3 - zh^2/12)\sin(\omega t)$. This function represents well the function plotted in Fig. 3(a). It passes through two extrema at $z = \pm h/(2\sqrt{3})$.

To test these theoretical predictions, I measured the mechanical impedance of a homeotropic nematic slab with a home-made piezoelectric rheometer.

III. EXPERIMENT

A. Setup

A full description of the piezoelectric rheometer can be found in Ref. [7]. This cell was designed to impose small thickness variations on a sample of controlled thickness h. Thanks to three differential screws and a linear variable differential transformer (LVDT, Shaevitz ATA-101), h can be continuously changed between ~ 0 and 1 mm with a 1-μm sensitivity and the parallelism between the two glass plates [of radii 0.5 cm (top plate) and 0.6 cm (bottom plate) and thickness 3 mm] can be adjusted to better than 1×10^{-4} rad. The cell is transparent in the middle and is mounted on the stage of a polarizing microscope, which allowed me to observe the sample and check the quality of the homeotropic anchoring after filling with the liquid crystal. The sample is regulated in temperature to within $\pm 0.01\,°$C thanks to two RKC HA400 controllers (one for each oven). The cell and the microscope are inside a Plexiglas box which is itself regulated at $22\,°$C to within $\pm 0.1\,°$C. In practice, the sample thickness h is measured to within ± 0.2 μm before filling with a spectrophotometer at a temperature T_{ref} close to the melting temperature of the nematic phase. If the temperature is changed after filling with the liquid crystal, the sample thickness is corrected to include the thermal dilation of the cell. This correction (measured with the spectrophotometer when the cell is empty) reads $h(T) = h(T_{\text{ref}}) - 0.168(T - T_{\text{ref}})$, where
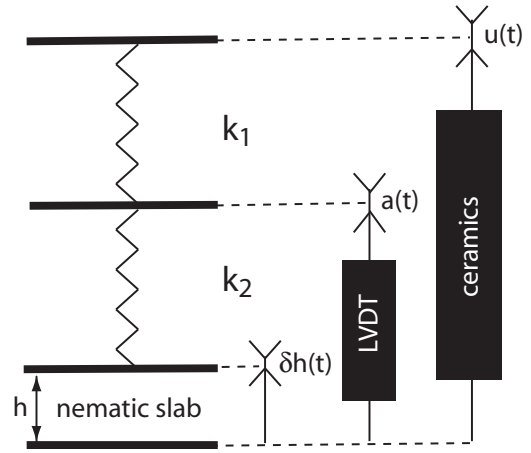
FIG. 4. Equivalent mechanical model of the cell.

h is given in micrometers and T in degrees Celsius. This correction turns out to be important when the samples are thin, which is the case in my experiment ($h \sim 20$ μm).

From a mechanical point of view, the cell is well modeled by two springs of force constants k_1 and k_2 in series with the sample (Fig. 4). In practice, the displacement $u(t)$ is imposed by three stacks of piezoelectric ceramics and the displacement $a(t)$ is measured with the LVDT. The ceramics are supplied with the internal function generator of a lock-in amplifier (Standford SR850), which is used to measure the displacements $u(t)$ and $a(t)$ and their phase shift ϕ. Sinusoidal deformations are used so that $u(t) = \sqrt{2}u_0 \sin(\omega t)$ and $a(t) = \sqrt{2}a_0 \sin(\omega t + \phi)$. In practice, we took care that the sample deformation $\delta h/h$ never exceeded 1×10^{-3}. Note the $\sqrt{2}$ factor used here as the lock-in amplifier gives rms values a_0 and u_0.

For an isotropic liquid of viscosity η the motion equations read

$$\begin{cases} \sigma = k_1(u - a) = k_2(a - \delta h), \\ \sigma = \dfrac{3}{2}\eta\dfrac{R^2}{h^2}\dfrac{\dot{\delta h}}{h}. \end{cases} \tag{31}$$

Solving these equations gives the amplitude ratio a_0/u_0 and the phase shift ϕ:

$$\begin{cases} \dfrac{a_0}{u_0} = \sqrt{\dfrac{\omega_r^2 + C^2\omega^2}{\omega_r^2 + (1 + C)^2\omega^2}}, \\ \tan(\phi) = -\dfrac{\omega\omega_r}{\omega_r^2 + C(1 + C)\omega^2}, \end{cases} \tag{32}$$

where $C = k_1/k_2$ is a rheometer parameter and ω_r a relaxation frequency

$$\omega_r = \frac{2k_1 h^3}{3R^2}\frac{1}{\eta}. \tag{33}$$

Note that ϕ passes through a minimum $\phi_{\min}$ given by

$$\tan(\phi_{\min}) = -\frac{1}{2\sqrt{C(C + 1)}} \tag{34}$$

at frequency

$$\omega_{\min} = \frac{\omega_r}{\sqrt{C(C+1)}}. \qquad (35)$$

An important point is that, with an isotropic liquid, $\phi_{\min}$ does only depend on C, independently of the value of the viscosity. Another point to mention is that $\phi \to 0$ when $\omega \to 0$. This is expected because, in this limit, $\sigma \to 0$ so that $a(t) \to u(t)$ according to Eq. (31). All this is to say that ϕ must not be confused with the phase shift between δh and the stress σ imposed on the sample.

These formulas can be generalized for a viscoelastic fluid of elastic and loss moduli G' and G''. A straightforward calculation yields

$$\begin{cases} \dfrac{a_0}{u_0} = \sqrt{\dfrac{(1+aC)^2\omega_r^2 + C^2\omega^2}{(1+a+aC)^2\omega_r^2 + (1+C)^2\omega^2}}, \\[4mm] \tan(\phi) = -\dfrac{\omega\omega_r}{(1+aC)(1+a+aC)\omega_r^2 + C(1+C)\omega^2}, \end{cases} \qquad (36)$$

where C is defined above and

$$a = \frac{3R^2}{k_1 h^3} G', \qquad (37)$$

$$\omega_r = \frac{2k_1 h^3}{3R^2} \frac{\omega}{G''}. \qquad (38)$$

These formulas are used to fit the experimental data. Again, we focus on the fact that $\phi \to 0$ when $\omega \to 0$, whatever the response of the sample, viscous or elastic.

B. Results

The liquid crystal chosen is 7CB (4-n-heptyl-4′-cyanobiphenyl). It was purchased at Frinton Laboratories (USA) and was used without further purification. The freezing range at the nematic-isotropic phase transition was of the order of 0.15 °C. The glass plates were treated with a silane compound to ensure strong homeotropic ordering. In practice the glass plates were successively cleaned with chromic-sulfuric acid, rinsed with distilled water, dipped in a HCl-water solution to remove all the chromium ions, rinsed again with distilled water, and finally placed in an oven at 120 °C overnight to dry. The plates were then dipped in a 1% silane (Merck ZLI-3124) solution dissolved in a mixture of extra dry toluene and 1,1,1-trichloroethane in the proportion of 1:1. After dipping, the plates were exposed to air for 15 min and then baked at 120 °C for half an hour. In this way, the humidity in the room catalyzes the hydrolyzation of the silane onto the glass, forming a covalent bond between silicon groups on the surface of the glass and that in the silane molecule. This method is known to give a very strong homeotropic anchoring [8]. The sample thickness at the solidus temperature $T_{NI} = 42.5$ °C of the nematic-isotropic phase transition was $h = 16.8$ μm.

I start with measurements in the isotropic liquid. Figure 5 shows raw experimental curves measured in the isotropic liquid at $\delta T = T - T_{NI} = 0.25$ °C (i.e., 0.1 °C above the liquidus temperature) when the voltage applied to the ceramics is of 2.5 Vrms. The first graph shows the blank signal u_0 measured before filling with the liquid crystal (it characterizes the response of the ceramics) and the signal a_0 measured
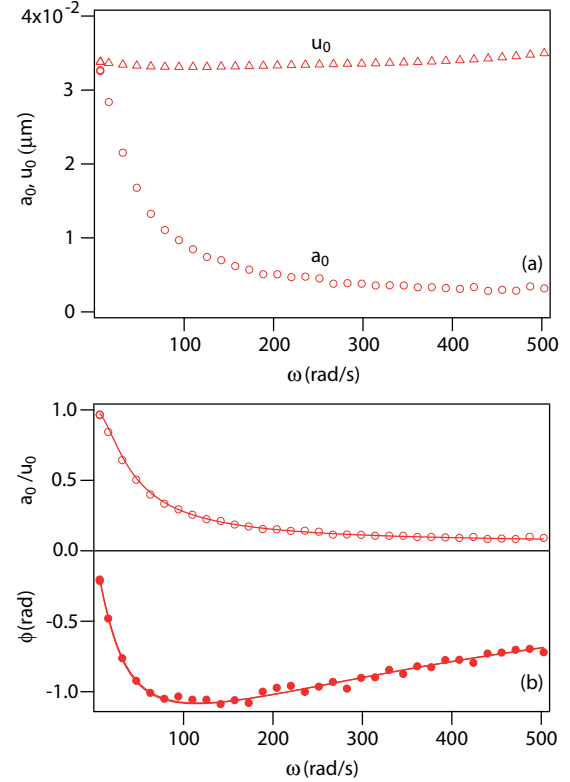
FIG. 5. (Color online) (a) Displacements u_0 and a_0 as a function of the angular frequency ω. The applied voltage is $V = 2.5$ Vrms. (b) Amplitude ratio a_0/u_0 and phase shift ϕ as a function of ω. The solid lines are the best fits of the data using Eqs. (32) and (33). Isotropic liquid, $\delta T = 0.25$ °C, $h = 16.7$ μm.

with the liquid crystal. The second graph shows the ratio a_0/u_0 and the phase shift ϕ between $a(t)$ and $u(t)$ (in phase with the applied voltage). These curves show that the sample deformation $\epsilon = \delta h / h < a_0/h$ never exceeds 1×10^{-3}. At this level, it is important to check that I am working in the linear regime of deformation. To this end, I measured u_0, a_0, and ϕ as a function of the applied voltage V at a fixed frequency (5 Hz, $\omega = 10\pi$ rad/s). The data given in Fig. 6 show that a_0 varies linearly with the applied voltage
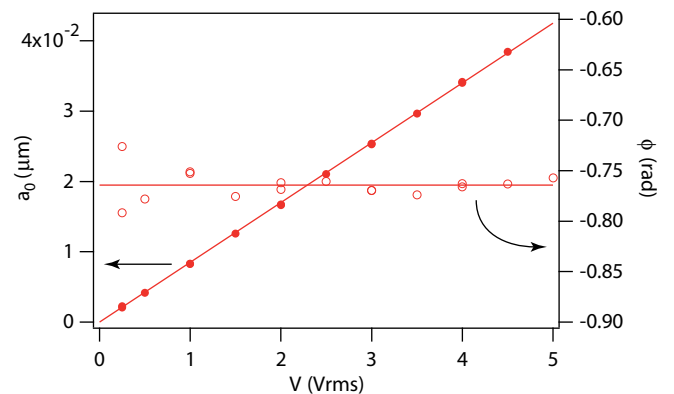
FIG. 6. (Color online) Displacement a_0 and phase shift ϕ as a function of the applied voltage V. Isotropic liquid, $\delta T = 0.25$ °C, $h = 16.7$ μm.
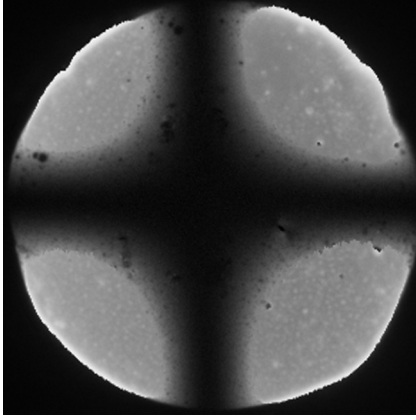
FIG. 7. Photo between crossed polarizers of the visible part of the sample. The photo was taken at small frequency (2 Hz, $\omega = 4\pi$ rad/s) when the contrast of the Maltese cross was a maximum. The hole diameter is 5 mm and the polarizers are parallel to the sides of the photo.

V while ϕ remains constant. This is the signature of the linear regime. This result also indicates that the meniscus effects are negligible (otherwise, the response of the sample would depend on the amplitude of the deformation). After these verifications, I can compare the experimental data to the model. To do so, the two curves $(a_0/u_0)(\omega)$ and $\phi(\omega)$ shown in Fig. 5(b) were fitted together (global fit) with the software IGOR PRO 6.12 (Wavemetrics, Inc., USA) by taking C and ω_r as free parameters in Eq. (36). This procedure gave $C = 0.0653 \pm 0.008$ and $\omega_r = 30.1 \pm 0.4$ rad/s. The viscosity was then obtained by taking $h = 16.8$ μm and $k_1 = 5.7 10^9$ Pa/m (this value was determined by performing similar measurements with oils of known viscosities). By assuming that h was known to within ± 0.2 μm (note that the thickness measurement is an important source of error here, for about one half of the total error) and by neglecting the error on k_1, I finally obtained $\eta = 0.0235 \pm 0.0012$ Pa s in very good agreement with the value given in Ref. [9]. Note that this viscosity corresponds to the co-called capillary viscosity of the isotropic phase [10]. Indeed, the frequencies used here are much too small to detect the de Gennes frequency corrections to the viscosity due to the short-range order effects present in the isotropic liquid just above the transition [3,11,12].

I now turn to the measurements in the nematic phase. First, I photographed with a camera equipped with a macrozoom lens the visible part of the sample between crossed polarizers. The observation was made in parallel light by closing as much as possible the aperture diaphragm of the objective. The observation of a Maltese cross (Fig. 7), which oscillates in intensity with a period double that of the excitation (this is expected as the phase shift between the ordinary and extraordinary rays, and consequently the transmitted intensity, is a function of n_r^2), shows that the flow-induced deformation of the director field is radial, as assumed in the calculation. Second, I measured the amplitude ratio a_0/u_0 and the phase shift ϕ between $a(t)$ and $u(t)$ in the nematic phase at various δT after having checked that I was still working in the linear regime of deformation. Three experimental curves are shown in Fig. 8 when $\delta T = -0.1°$, $-5°$, and $-15°$C. It is noteworthy
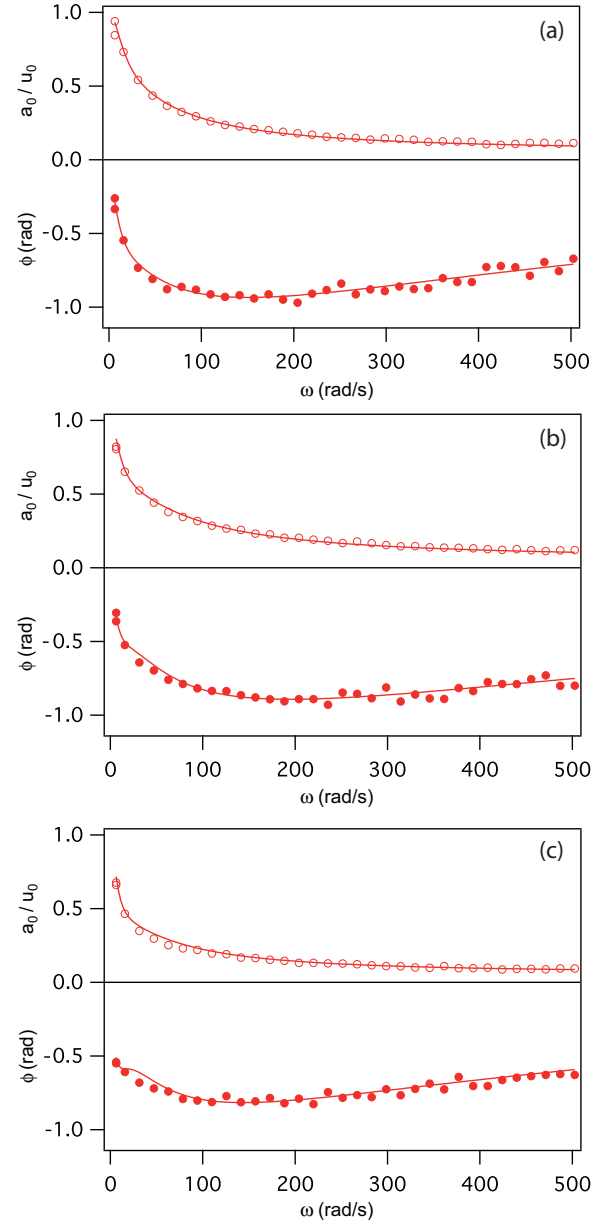
FIG. 8. (Color online) Amplitude ratio and phase shift as a function of the angular frequency in the nematic phase at three different temperatures: (a) $\delta T = -0.1$ °C, $h = 16.8$ μm; (b) $\delta T = -5$ °C, $h = 17.6$ μm; and (c) $\delta T = -15$ °C, $h = 19.3$ μm. The solid lines are the best fits of the data to the complete model.

here that ϕ systematically passes through a minimum, the value of which is higher than that predicted by Eq. (34) (of the order of -1.1). This result shows that the experimental curves obtained in the nematic phase cannot be correctly fitted with the model for an isotropic liquid. By contrast, the experimental curves are well fitted by using Eqs. (36)–(38) and the exact expressions (25), (28), and (29) for G' and G'', as shown in Fig. 8. This directly shows that the nematic sample is viscoelastic. Here again, I performed a global fit of the two curves at each temperature by fixing the value of C at 0.0653 (this is the value found when the rheometer is filled with an isotropic liquid) and by choosing as free parameters the
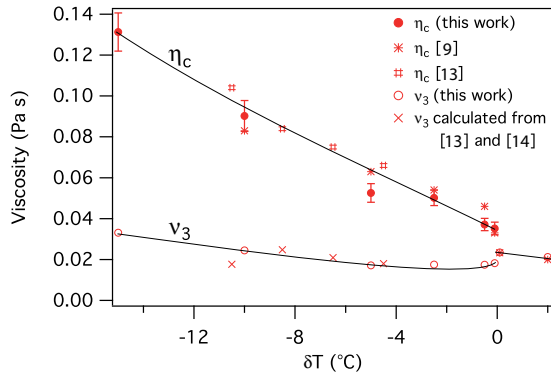
FIG. 9. (Color online) Viscosities as a function of temperature. For ν_3, the error bars are not reported because the error is of the order of the size of the open circles. The values of ν_3 corresponding to the crosses have been calculated from the values of η_c and α_2 given in Ref. [13] and the value of γ_1 given in Ref. [14]. The solid lines are guides to the eye.

FIG. 10. (Color online) Diffusivity as a function of temperature. The solid line is a guide for the eye.

diffusivity D and the two viscosities η_c and ν_3 (or equivalently $k\alpha_2$ and ν_3). This procedure led to viscosities shown in Fig. 9 and the diffusivity shown in Fig. 10. Again, the errors were calculated by assuming that, at each temperature, the sample thickness (corrected for the temperature drift) was known to within ± 0.2 μm. Values of η_c and D obtained from the literature were also reported in these figures (with η_c taken from Refs. [9,13] while D and k, and so ν_3, were calculated from values of K_3 given in Ref. [15], and values of γ_1 given in Ref. [14]) and values of η_c and α_2 given in Ref. [13]. This comparison shows that the present values of η_c and ν_3 agree well with those of the literature within the experimental errors.

IV. CONCLUSION

This study shows that a homeotropic nematic slab has a viscoelastic behavior under (dilation-compression) sinusoidal deformation. The prediction of Okano *et al.* [1], namely, that the slab behaves as an isotropic liquid of viscosity η_c, is only valid at low frequency with respect to D/h^2. At larger frequency, the nematic slab rather behaves as an isotropic liquid of viscosity ν_3. It is in this regime that the

experiment of Yamamoto and Okano [2] was in fact conducted. With my rheometer, these two regimes are difficult to reach. Yet this is rather an advantage because measuring in the intermediate regime—where G' and G'' are of the same order of magnitude—enabled me to simultaneously obtain the orientational diffusivity $D = K_3/\gamma_1$ and the two viscosities η_c and ν_3. Another advantage of this measurement is that there is no need to impose a strong electric or magnetic field to orient the director under flow, which is necessary to directly measure the viscosity η_c [9]. Last but not least, I detected neither viscoelastic behavior nor induced birefringence in the isotropic liquid just above the transition, unlike the recent measurements of Kahl *et al.* [16,17]. This could be due to the lack of sensitivity of my rheometer which was primarily designed to study much more viscous fluids such as smectic phases [7] or, more likely, to the wetting conditions of the nematic phase on the plates which are different from those used in Refs. [16,17].

[1] K. Okano and J. Yamamoto, Mechanical transfer function of thin smectic A slab having homeotropic structure, Jpn. J. Appl. Phys. **29**, 1149 (1990).

[2] J. Yamamoto and K. Okano, Anomalous hydrodynamic behaviors of smectic liquid crystals at low frequencies, Jpn. J. Appl. Phys. **30**, 754 (1991).

[3] P. G. de Gennes, *The Physics of Liquid Crystals* (Clarendon Press, Oxford, UK, 1975), p. 75.

[4] P. Oswald and P. Pieranski, *Nematic and Cholesteric Liquid Crystals: Concepts and Physical Properties Illustrated by Experiments* (CRC Press, Boca Raton, FL, 2005).

[5] P. C. Martin, O. Parodi, and P. J. Pershan, Unified hydrodynamic theory for crystals, liquid crystals, and normal fluids, Phys. Rev. A **6**, 2401 (1972).

[6] P. Oswald, *Rheophysics: The Deformation and Flow of Matter* (Cambridge University Press, Cambridge, UK, 2009), p. 354.

[7] P. Oswald and D. Le Fur, Réalisation d'une cellule de déformation adaptée à l'étude des cristaux liquides smectiques, C. R. Acad. Sci. Paris **297**, 699 (1983).

[8] F. J. Kahn, Orientation of liquid crystals by surface coupling agents, Appl. Phys. Lett. **22**, 386 (1972).

[9] J. Ananthaiah, Rasmita Sahoo, M. V. Rasna, and Surajit Dhara, Rheology of nematic liquid crystals with highly polar molecules, Phys. Rev. E **89**, 022510 (2014).

[10] P. Martinoty, F. Kiry, S. Nagai, and S. Candau, Viscosity coefficients in the isotropic phase of a nematic liquid crystal, J. Phys. (Paris) **38**, 159 (1977).

[11] P. G. de Gennes, Phenomenology of short-range-order effects in the isotropic phase of nematic materials, Phys. Lett. A **30**, 454 (1969).

[12] P. G. de Gennes, Short range order effects in the isotropic phase of nematics and cholesterics, Mol. Cryst. Liq. Cryst. **12**, 193 (1971).

[13] P. Patricio, C. R. Leal, L. F. V. Pinto, A. Boto, and M. T. Cidade, Electro-rheology study of a series of liquid crystal cyanobiphenyls: Experimental and theoretical treatment, Liq. Cryst. **39**, 25 (2012).

[14] P. Oswald, G. Poy, F. Vittoz, and V. Popa-Nita, Experimental relationship between surface and bulk rotational

viscosities in nematic liquid crystals, Liq. Cryst. **40**, 734 (2013).

[15] N. V. Madhusudana and R. Prathiba, Elasticity and orientational order in some cyanobiphenyls: Part IV. Reanalysis of the data, Mol. Cryst. Liq. Cryst. **89**, 249 (1982).

[16] P. Kahl, P. Baroni, and L. Noirez, Hidden solidlike properties in the isotropic phase of the 8CB liquid crystal, Phys. Rev. E **88**, 050501(R) (2013).

[17] P. Kahl, G. Baroni, and L. Noirez, Harmonic strain-optical response revealed in the isotropic (liquid) phase of liquid crystals, Appl. Phys. Lett. **107**, 084101 (2015).